

Deep learning for clustering of continuous gravitational wave candidates II: identification of low-SNR candidates

B. Beheshtipour^{1, 2, a} and M.A. Papa^{1, 2, 3, b}

¹*Max Planck Institute for Gravitational Physics (Albert Einstein Institute), Callinstrasse 38, 30167 Hannover, Germany*

²*Leibniz Universität Hannover, D-30167 Hannover, Germany*

³*University of Wisconsin Milwaukee, 3135 N Maryland Ave, Milwaukee, WI 53211, USA*

Broad searches for continuous gravitational wave signals rely on hierarchies of follow-up stages for candidates above a given significance threshold. An important step to simplify these follow-ups and reduce the computational cost is to bundle together in a single follow-up nearby candidates. This step is called clustering and we investigate carrying it out with a deep learning network. In our first paper [1], we implemented a deep learning clustering network capable of correctly identifying clusters due to large signals. In this paper, a network is implemented that can detect clusters due to much fainter signals. These two networks are complementary and we show that a cascade of the two networks achieves an excellent detection efficiency across a wide range of signal strengths, with a false alarm rate comparable/lower than that of methods currently in use.

I. INTRODUCTION

The detection of gravitational waves from binary mergers represents a historical breakthrough and opened the new era of gravitational wave astronomy [2–4]. Continuous gravitational waves are ever-lasting nearly monochromatic gravitational waves which have not yet been detected, most probably due to their weakness [5–9]. They are expected from isolated rotating compact objects when their shape or motion deviates from perfect axisymmetry [10–13].

Broad-frequency surveys are routinely carried out [14–16], which investigate a very large number – $O(10^{17})$ – of possible waveforms, and require a so-called “clustering” of the initial results.

Why is clustering important? A gravitational wave signal or a disturbance may trigger not only one template but a number of nearby templates, to rise above the average noise level. This produces many “candidates”, each needing to be followed up and resulting in a high computing cost. To keep the computing cost in check one could increase the threshold that the detection statistic of a candidate has to exceed in order to be worthy of follow-up. But this obviously results in a loss of sensitivity. To tip the balance towards higher sensitivities at the same computing cost, clustering is used.

Clustering identifies nearby candidates due to the same root-cause and bundles them together as one. Only the most significant candidate of the set is followed-up and this reduces the computational cost.

Clustering algorithms used in broad continuous waves surveys have evolved over time [17–20]. The main difficulty of clustering lies in the fact that the mismatch reduction function can be computed analytically only at distances from the signal parameters that are much smaller than those at which signal clusters from actual

searches extend. This makes it necessary to resort to extensive Monte Carlos in order to determine the parameters of all deterministic clustering approaches.

In our first paper [1] we explored the idea of using the computational cost normally used for the tuning Monte Carlos, to generate search results with clusters from simulated signals and to train a deep learning neural network on these.

Deep learning or deep neural networks are a subfield of machine learning which is inspired by the way brain works. A network consists of layers of nodes/neurons that endeavour to recognize features in the input data. Neural networks have proven successful in many applications, including ones in gravitational waves physics: noise studies and de-noising [21–24], detection of binary spiral signals and estimation of their parameters [25–31]. Recently [32–34] have proposed to use deep neural networks for detecting continuous gravitational waves. See [35] for a review.

We begun the clustering-network development in [1] tackling the simpler clustering problem, that is to cluster candidates from loud signals. We now want to explore the clustering of weaker signals.

The paper is organized as follows. In Section II we recall what the general context is, for gravitational wave search results from broad surveys, and we concentrate on the broadest existing surveys, i.e. the Einstein@Home ones. In Section III we present the new network, capable of detecting weak-signal clusters; in Section IV we discuss a composite network. Finally in Section V we recap the main results, and compare and contrast the performance of our newly developed clustering schemes with existing methods.

II. GRAVITATIONAL WAVE SEARCH RESULTS

We develop and benchmark our clustering method on the results of the latest Einstein@Home all-sky search

^a b.beheshtipour@aei.mpg.de

^b maria.alessandra.papa@aei.mpg.de

[16]. This search utilises public data from the LIGO O2 run [36, 37] spanning about 9 months, covers a signal-frequency f between 20 Hz and ≈ 600 Hz, spin-down \dot{f} between -2.6×10^{-9} Hz/s and 2.6×10^{-10} Hz/s and has a typical set-up for such parameter space.

An Einstein@Home search [38] splits the computational workload in to millions of separate work-units and distributes them among the volunteer computers. Each work-unit searches just under 10^{11} different waveforms corresponding to a 50 mHz band in frequency, the entire spin down range, and a small patch of the sky. The central Einstein@Home server receives back information only about the most significant 7500 of these waveforms. We refer to these as candidates. A candidate comprises a value of the detection statistics, and a set of template parameter: $f, \dot{f}, \alpha, \delta$.

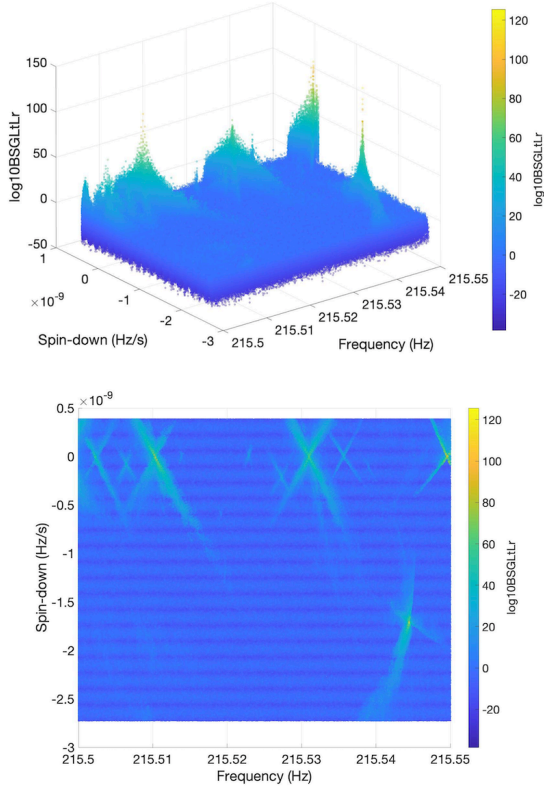


FIG. 1. Results from the Einstein@Home search in the 215.50 – 215.55 Hz band; the detection statistic as a function of f and \dot{f} is shown. Fake signals appear in this result-set as parameter space regions with enhanced values of the detection statistic. The lower plot displays the top-down view.

Figure 1 shows the results in the 215.50 – 215.55 Hz band as a function of the candidates’ frequency and spin-down, with the detection statistic value color-coded. Several X-shaped areas are evident that present high values of the detection statistic: these are due to fake signals added to the data before the search. These are the structures that we want to cluster. The input data to our

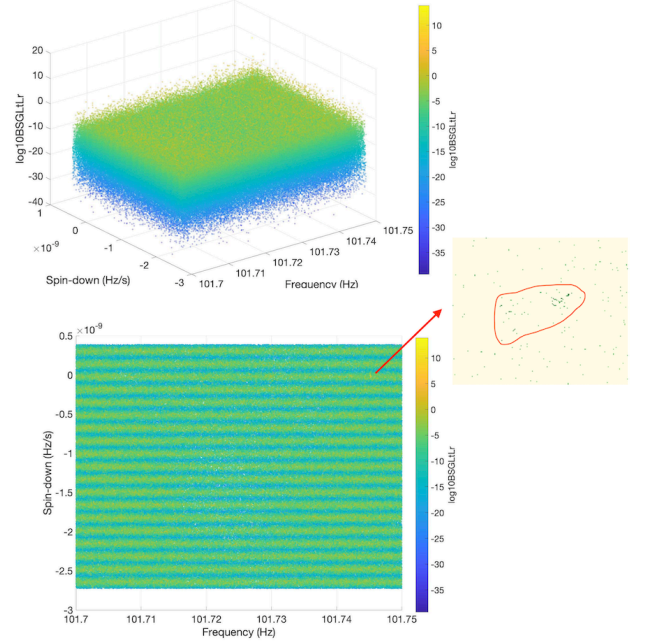


FIG. 2. Results from the Einstein@Home search in the 101.70 – 101.75 Hz band; the detection statistic as a function of f and \dot{f} is shown. These plots are similar to those shown in Fig 1, apart for the fact that here we show a weak signal, like those targeted by the WeakSigN. The zoomed-in panel shows the ground-truth cluster region.

network can be broadly thought of, as images like this.

III. THE WEAK-SIGNAL NETWORK

A. Target signals

In [1] we developed a network that could cluster search results from loud signals. We refer to this network as the loud-signal-network (LoudSigN). The detection efficiency of this network drops to less than 17% for signals with detection statistic $\hat{\beta}_{S/GLtLr} \sim 20$, and this is inadequate for the level of sensitivity of the latest searches: in [16] nearly all candidates that are followed-up have $\hat{\beta}_{S/GLtLr}$ values lower than 20.

We recall that the input data for the large-signal-network is “down-sampled”: the resolution of the original $f - \dot{f}$ images is reduced by averaging over a certain number of pixels, 12×12 for the O2 data. This is a necessary step because it blurs away the structure of local “peaks and valleys” making it easier for a network to clump everything together as a single cluster. On the other hand this step also decreases the contrast of the signal peak, and if the signal is weak enough, this step blurs it away completely.

We design a network aimed at these weaker signals. We

define these signals as those that would not be visible in the input data prepared for the loud-signal-network, but that are visible or barely visible in the original O2 data. We refer to this new network as the weak-signal-network (WeakSigN). Figure 2 shows an example of a weak target signal.

B. Input data and ground truth

The input to the network are images with 512×512 pixels, that can be handled by the high-end 32 GB GPU. In this result-set they correspond to slices of $1.7 \text{ mHz} \times 1.7 \times 10^{-7} \text{ Hz/s}$.

As the Einstein@Home results only include top templates in detection statistics, we have many empty pixels in an image. Also it is possible to have more than one candidate for each f, \dot{f} pixel, corresponding to different sky positions. In such cases, the candidate with the highest detection statistic value is picked.

We use a supervised network that, with each training input needs the corresponding output, called ground truth. Here the ground truth is a matrix for each image that identifies the pixels that are part of a cluster. To generate the ground truth, we identify the clusters by eye and mark them using an image editing tool (Pixelmator) on a tablet computer equipped with a touchscreen. Each region is saved with the editing tool and then converted to the ground truth matrix. An example is given in the zoomed-in panel of Figure 2.

C. The network

The clustering method is addressed by using instance segmentation networks. The general network architecture, the overall gravitational data structure, and preparation of the input data set for the network is similar to [1]. Here we mostly concentrate on the key points, improvements and differences and refer the reader to [1] for more details.

The network scans the image and finds the regions that most likely include the cluster, then classifies them and generates definitive boundaries. The output is a pixel mask that determines the boundaries and a score that identifies how likely a pixel is part of a signal cluster. The score threshold that decides whether a pixel is or not part of a cluster is set at 0.5. The network structure is summarized in Figure 3.

To train the network, there are several parameters that need to be adjusted such as model weights, batch size, etc. When an input is given to a network node, it applies a linear function with a set of coefficients and biases, called model-weights. In this paper, the starting model-weights are set to be the weights from trained network in [1]. Another important parameter is batch size which is mainly limited by the size of the GPU memory. In training a network, the input data is divided into several

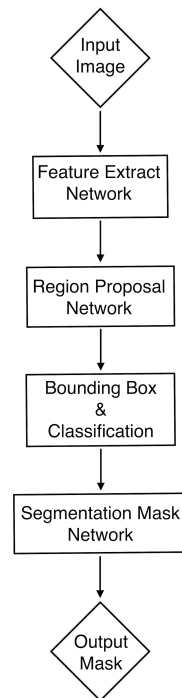


FIG. 3. A schematic diagram of the Mask R-CNN architecture used for our clustering networks.

batches with a size defines with the batch size parameter. The network works through all samples in each batch before updating the network weights. In [1], a large batch size of 15 made a big improvement in the network performance because the network started from pre-trained model weights that were not for this specific problem. Here starting with model-weights from [1] helps to significantly lower the batch size without loosing in performance and at the same time frees up some memory to use a bigger size sub-image. Having bigger sub-images gives a better picture of the clustered structures over the background noise that they are embedded in. For this network we use a batch size of 2 with sub-images of 512×512 while in [1] the batch size was 15 with sub-images of size 256×256 .

Similar to [1], the training is performed in 3 steps which proved to enhance performance. Since we begin with more reliable weights, the first two training steps can be made shorter compared with [1]. The steps are as follows: 1) only the first layer of the three last levels in Figure 3 are trained, for 60 epochs rather than 100 epochs in [1] 2) using the weights from the previous step, the first three levels are trained for 120 epochs rather than 300 epochs as in [1] 3) the complete network is trained with the weights from the second step for 1000 epochs. The best performance of the network is achieved with these hyper-parameters: learning rate=0.001, weight decay=0.00001, learning momentum=0.9. The training process takes about 40 hours to complete.

D. Results

The network is trained on 518 sub-images, validated on 218 sub-images, and tested on 515 sub-images. The test-set contains the 218 validation-set images plus 297 new sub-images. All these sets only include clusters which are weak as described in Section III A. The test set includes 515 signal clusters of which the network correctly identifies 452, corresponding to 88% detection efficiency. The detection efficiency as a function of the normalized signal amplitude is shown in Figure 4. We define the normalized amplitude for a signal at frequency f with intrinsic amplitude h_0 the ratio $h_0/\sqrt{S_h(f)}$, where $S_h(f)$ is the power spectra density at that frequency. The cosine of the inclination angle and the polarization angle for the population of signals are distributed uniformly between -1 and 1 and $-\pi/4$ and $\pi/4$, respectively. We note that the normalized amplitude is the inverse of the sensitivity depth that a search should reach in order to detect this population of signals.

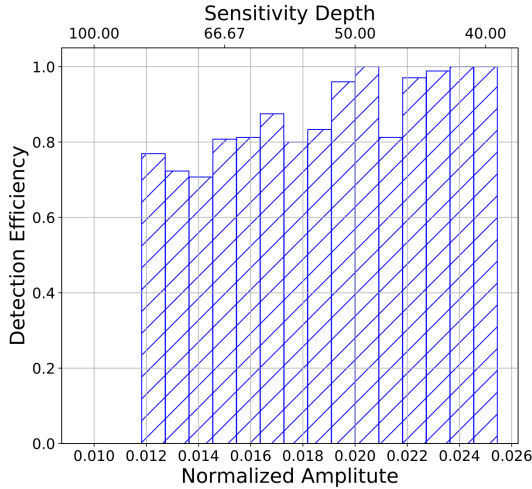


FIG. 4. Detection efficiency of the WeakSigN as a function of fake signal normalized amplitude.

The WeakSigN does not perform as well on loud signals. Clusters from loud signals typically spread over more than a single sub-image and present structures. The network picks up parts of these structures as being small clusters, which generates a higher rate of false alarms around loud signals and disturbances. Perhaps more importantly the network misses the general picture. We show an example of this in Figure 5, where the network does not even return a cluster that contains the signal parameters.

IV. THE CASCADE-NETWORK

We investigate the combination of the LoudSigN and the WeakSigN to efficiently detect signal clusters over

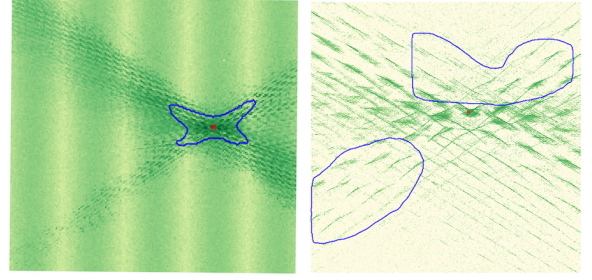


FIG. 5. Performance of WeakSigN (right image) and LoudSigN (left image) on one loud signal cluster at frequency of 459.035 Hz. The blue lines show the detection boundaries of the clusters found by the network and the red cross shows the injection. Left image shows the signal cluster in low-resolution image and the right image shows this cluster in high-resolution image. The LoudSigN observed one region contained the signal cluster while the WeakSigN detected 2 clusters for that.

a broad range of signal amplitudes. We re-train the LoudSigN of [1] on the O2 data and we use it on the O2 data. We record the clusters identified by this network and set the corresponding pixels to “empty” in the original image. The resulting image is fed to the WeakSigN. We record the clusters identified by the WeakSigN.

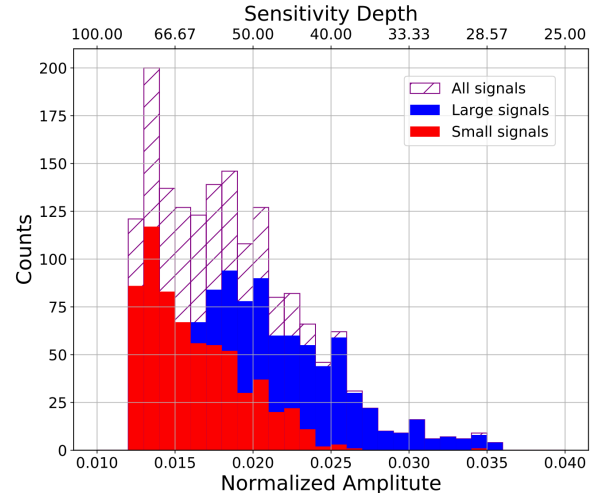


FIG. 6. Distribution of the normalized gravitational wave amplitudes of the fake signals used to characterise the performance of the cascade-network. The different colours shows how the signal appeared in the search output, i.e. whether it gave rise to a loud cluster or a weak cluster.

We characterize the performance of the cascade-network on 1684 fake signals in the frequency range 40-579 Hz and having a wide range of signal strengths, as shown in Figure 6. We consider a signal detected when the cluster contains at least a candidate from the signal. It may happen that the first network identifies part of a signal cluster, and the second network picks-up weaker candidates. In this case the same injection is associated

with a cluster in each network. Figure 7 shows the efficiency in detecting the clusters associated to the injected signal, as a function of the signal strength.

We find that all clusters with normalized signal amplitude of $\gtrsim 1/40$ are detected and that the network has a detection efficiency of more than 95% up to signal strengths of $\approx 1/54$. For weaker signals the new network significantly contributes to the detection efficiency and at $\approx 1/80$ accounts for more than half of the detected signals.

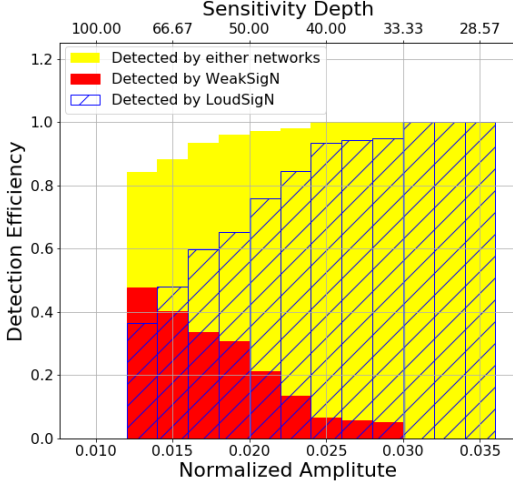


FIG. 7. Top: Detection efficiency of the cascade method network. The distribution of each network is shown in different colours.

We evaluate the uncertainty in signal parameters that we'd assign to each candidate identified by the network. We use the results from the fake signals studies as follows: We find the candidate corresponding to the highest value of the detection statistic in each signal cluster, and calculate the distance to the actual signal parameters. If more than a cluster exists associated with the same fake signal, for the purposes of evaluating this distance, we consider the cluster that is closest to the signal. Figure 8 shows the cumulative rate of candidates within a given f, \dot{f} distance of the actual signal parameters. Our results indicate an uncertainty region of 4.5×10^{-4} Hz and 6.8×10^{-11} Hz/s for cluster from the LoudSigN and of 6.5×10^{-4} Hz and 7.4×10^{-11} Hz/s for clusters identified by the WeakSigN.

We evaluate the false alarm rate of the cascade-network by running it on the Einstein@Home O2 result-set [16]. We randomly pick 1777 50-mHz frequency bands over the entire search range and apply the cascade-network to the results from these bands. The false alarm rate is dominated by the LoudSigN and the WeakSigN shows a negligible false alarm rate. As shown in Figure 10, the false alarm rate of the cascade network is not constant in frequency. The higher false alarm in the middle frequency range stems from features in the result-set, which are

more visible in the middle-range bands.

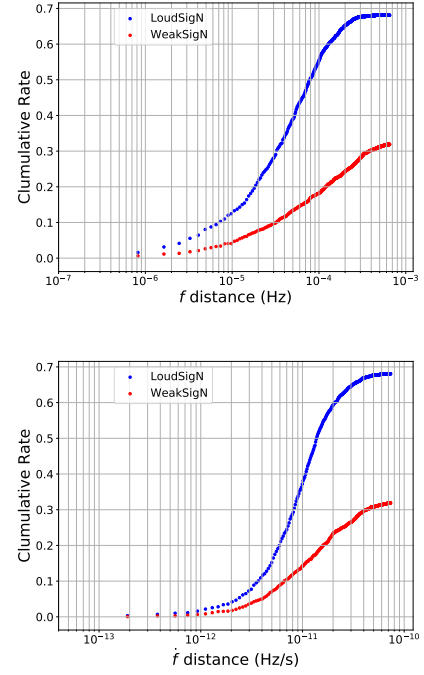


FIG. 8. Cumulative distribution of the distance between the signal parameters and the parameters of the most significant cluster candidate (the candidate with the highest detection statistics value) recovered by the network. The top plot shows the distance in frequency; the bottom plot the distance in spin-down (right).

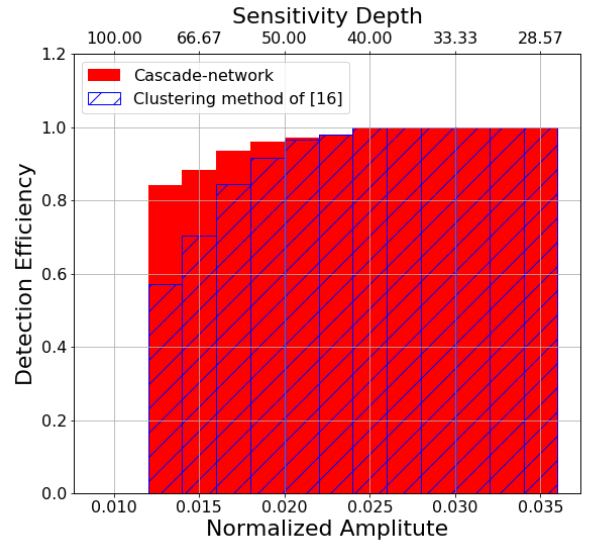


FIG. 9. Comparing the cascade-network with the deterministic clustering method used in the analysis of the Einstein@Home search results [16]. Our network shows a higher detection efficiency for lower amplitude signals.

Overall our cascade network generates half the false alarms than the clustering method employed in the latest Einstein@Home all-sky search on the same bands [16].

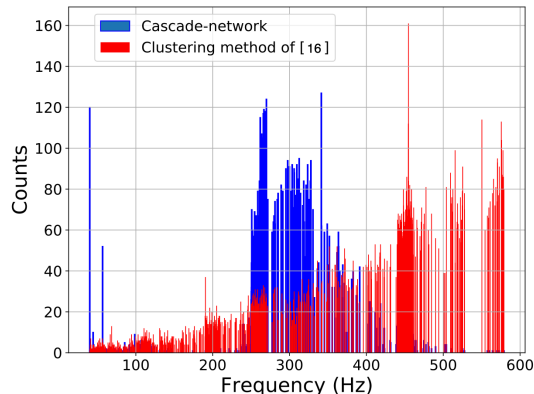


FIG. 10. False alarm rate versus signal frequency for our network and for the clustering method used in [16].

V. CONCLUSION

In [1] we presented the first deep learning network trained to identify signal clusters in the output of very broad searches for continuous wave signals. That network was aimed at large signals. In this paper we build on this and design a second network that is capable of identifying clusters from faint signals. We train and test the network on the most recent results from an all-sky Einstein@Home search of LIGO O2 data [16]. We show that a cascade-architecture of these two networks can identify clusters of continuous gravitational wave signal candidates over a broad range of signal strengths.

The cascade-network shows an excellent performance, with a detection efficiency of 92% above normalised signal amplitudes of $1/60$. This exceeds the performance of the deterministic clustering method used in [16] which has a detection efficiency of 83% in that amplitude range. For weak signals – at normalised amplitudes of $1/80$ – our cascade-network maintains a detection efficiency of $\gtrsim 80\%$ whereas the deterministic clustering performance drops to less than 50%. Figure 9 summarises the perfor-

mance comparison.

Over a broad frequency range the overall false alarm rate of our cascade-network is half that of [16], albeit with peaks up to four times larger than [16] between 250 Hz and 350 Hz. Since these false alarms are due to features in the results-set, we are confident that a tweak to the method to account with this peculiarity could be implemented and it would reduce the false alarm rate in this band.

The uncertainty in f and \dot{f} of our network is competitive, being 1.68 and 1.25 times smaller than the uncertainties of the clustering method used in [16].

As explained earlier on, each template is identified by a sky location as well as a f and \dot{f} value. While we simplified our clustering to f and \dot{f} , the question naturally arises of how well the network identifies the sky position of a signal. The uncertainty in the sky by LoudSigN is \approx half that of the deterministic clustering method; but the sky-uncertainty of the WeakSigN is much larger than that of the deterministic clustering method, in occasions yielding seemingly unrelated sky positions. In this respect the sky-localisation performance of the cascade network falls short of optimal. A possible next step is to design the single networks to work directly in 4D and to consider not only the candidates' detection statistic, but also their local density.

VI. ACKNOWLEDGMENTS

We thank Benjamin Steltner for providing the performance benchmark data for the clustering procedure used in [16]. The computing work for this project was carried out on the GPUs of the Atlas cluster of the Observational Relativity and Cosmology division of the MPI for Gravitational Physics, Hannover [39]. We thank Bruce Allen for supporting this project by granting us access to those systems.

This research has made use of search results from LIGO data from the LIGO Open Science Center (<https://losc.ligo.org>), a service of LIGO Laboratory, the LIGO Scientific Collaboration and the Virgo Collaboration. LIGO is funded by the U.S. National Science Foundation. Virgo is funded by the French Centre National de Recherche Scientifique (CNRS), the Italian Istituto Nazionale della Fisica Nucleare (INFN) and the Dutch Nikhef, with contributions by Polish and Hungarian institutes.

-
- [1] B. Beheshtipour and M. A. Papa, Deep learning for clustering of continuous gravitational wave candidates, *Phys. Rev. D* **101**, 064009 (2020), arXiv:2001.03116 [gr-qc].
 - [2] B. Abbott, R. Abbott, T. Abbott, M. Abernathy, F. Acernese, K. Ackley, C. Adams, T. Adams, P. Addesso, R. Adhikari, and et al., Observation of gravitational waves from a binary black hole merger, *Physical Review*

- Letters* **116**, 10.1103/physrevlett.116.061102 (2016).
- [3] A. H. Nitz, C. Capano, A. B. Nielsen, S. Reyes, R. White, D. A. Brown, and B. Krishnan, 1-oggc: The first open gravitational-wave catalog of binary mergers from analysis of public advanced ligo data, *The Astrophysical Journal* **872**, 195 (2019).
- [4] B. Abbott, R. Abbott, T. Abbott, S. Abraham, F. Acer-

- nese, K. Ackley, C. Adams, R. Adhikari, V. Adya, C. Affeldt, and et al., Gwtc-1: A gravitational-wave transient catalog of compact binary mergers observed by ligo and virgo during the first and second observing runs, *Physical Review X* **9**, 10.1103/physrevx.9.031040 (2019).
- [5] P. D. Lasky, Gravitational waves from neutron stars: A review, *Publications of the Astronomical Society of Australia* **32**, 10.1017/pasa.2015.35 (2015).
- [6] B. P. Abbott, R. Abbott, T. D. Abbott, S. Abraham, F. Acernese, K. Ackley, C. Adams, R. X. Adhikari, V. B. Adya, C. Affeldt, and et al., Searches for gravitational waves from known pulsars at two harmonics in 2015–2017 ligo data, *The Astrophysical Journal* **879**, 10 (2019).
- [7] B. Abbott, R. Abbott, T. Abbott, S. Abraham, F. Acernese, K. Ackley, C. Adams, R. Adhikari, V. Adya, C. Affeldt, and et al., All-sky search for continuous gravitational waves from isolated neutron stars using advanced ligo o2 data, *Physical Review D* **100**, 10.1103/physrevd.100.024004 (2019).
- [8] V. Dergachev and M. A. Papa, Results from an extended falcon all-sky survey for continuous gravitational waves (2019), arXiv:1909.09619 [gr-qc].
- [9] V. Dergachev and M. A. Papa, Sensitivity improvements in the search for periodic gravitational waves using o1 ligo data, *Physical Review Letters* **123**, 10.1103/physrevlett.123.101101 (2019).
- [10] B. Haskell, R-modes in neutron stars: Theory and observations, *International Journal of Modern Physics E* **24**, 1541007 (2015).
- [11] A. Singh, Gravitational wave transient signal emission via ekman pumping in neutron stars during post-glitch relaxation phase, *Physical Review D* **95**, 10.1103/physrevd.95.024022 (2017).
- [12] G. Walin, Some aspects of time-dependent motion of a stratified rotating fluid, *Journal of Fluid Mechanics* **36**, 289–307 (1969).
- [13] M. Abney and R. I. Epstein, Ekman pumping in compact astrophysical bodies, *Journal of Fluid Mechanics* **312**, 327–340 (1996).
- [14] J. Ming et al., Results from an Einstein@Home search for continuous gravitational waves from Cassiopeia A, Vela Jr. and G347.3, *Phys. Rev. D* **100**, 024063 (2019), arXiv:1903.09119 [gr-qc].
- [15] M. A. Papa, J. Ming, E. V. Gotthelf, B. Allen, R. Prix, V. Dergachev, H.-B. Eggenstein, A. Singh, and S. J. Zhu, Search for Continuous Gravitational Waves from the Central Compact Objects in Supernova Remnants Cassiopeia A, Vela Jr., and G347.3–0.5, *Astrophys. J.* **897**, 22 (2020), arXiv:2005.06544 [astro-ph.HE].
- [16] B. Steltner, M. A. Papa, H. B. Eggenstein, B. Allen, V. Dergachev, R. Prix, B. Machenschalk, S. Walsh, S. J. Zhu, and S. Kwang, Einstein@Home all-sky search for continuous gravitational waves in LIGO O2 public data, arXiv e-prints , arXiv:2009.12260 (2020), arXiv:2009.12260 [astro-ph.HE].
- [17] B. Steltner, M. A. Papa, and etc., Density-clustering of gravitational wave candidates from large surveys, .
- [18] B. Behnke, M. A. Papa, and R. Prix, Postprocessing methods used in the search for continuous gravitational-wave signals from the galactic center, *Physical Review D* **91**, 10.1103/physrevd.91.064007 (2015).
- [19] M. A. Papa, H.-B. Eggenstein, S. Walsh, I. Di Palma, B. Allen, P. Astone, O. Bock, T. D. Creighton, D. Keitel, B. Machenschalk, and et al., Hierarchical follow-up of subthreshold candidates of an all-sky einstein@home search for continuous gravitational waves on ligo sixth science run data, *Physical Review D* **94**, 10.1103/physrevd.94.122006 (2016).
- [20] A. Singh, M. A. Papa, H.-B. Eggenstein, and S. Walsh, Adaptive clustering procedure for continuous gravitational wave searches, *Physical Review D* **96**, 10.1103/physrevd.96.082003 (2017).
- [21] M. Razzano and E. Cuoco, Image-based deep learning for classification of noise transients in gravitational wave detectors, *Classical and Quantum Gravity* **35**, 095016 (2018).
- [22] D. George, H. Shen, and E. Huerta, Classification and unsupervised clustering of ligo data with deep transfer learning, *Physical Review D* **97**, 10.1103/physrevd.97.101501 (2018).
- [23] H. Shen, D. George, E. A. Huerta, and Z. Zhao, Denoising gravitational waves using deep learning with recurrent denoising autoencoders (2017), arXiv:1711.09919 [gr-qc].
- [24] W. Wei and E. Huerta, Gravitational wave denoising of binary black hole mergers with deep learning, *Physics Letters B* **800**, 135081 (2020).
- [25] X. Fan, J. Li, X. Li, Y. Zhong, and J. Cao, Applying deep neural networks to the detection and space parameter estimation of compact binary coalescence with a network of gravitational wave detectors, *Science China Physics, Mechanics & Astronomy* **62**, 10.1007/s11433-018-9321-7 (2019).
- [26] H. Shen, E. A. Huerta, Z. Zhao, E. Jennings, and H. Sharma, Deterministic and bayesian neural networks for low-latency gravitational wave parameter estimation of binary black hole mergers (2019), arXiv:1903.01998 [gr-qc].
- [27] T. D. Gebhard, N. Kilbertus, I. Harry, and B. Schölkopf, Convolutional neural networks: A magic bullet for gravitational-wave detection?, *Physical Review D* **100**, 10.1103/physrevd.100.063015 (2019).
- [28] D. George and E. Huerta, Deep neural networks to enable real-time multimessenger astrophysics, *Physical Review D* **97**, 10.1103/physrevd.97.044039 (2018).
- [29] H. Gabbard, M. Williams, F. Hayes, and C. Messenger, Matching matched filtering with deep networks for gravitational-wave astronomy, *Physical Review Letters* **120**, 10.1103/physrevlett.120.141103 (2018).
- [30] Y.-C. Lin and J.-H. Protty Wu, Detection of Gravitational Waves Using Bayesian Neural Networks, arXiv e-prints , arXiv:2007.04176 (2020), arXiv:2007.04176 [astro-ph.IM].
- [31] M. B. Schäfer, F. Ohme, and A. H. Nitz, Detection of gravitational-wave signals from binary neutron star mergers using machine learning, *Phys. Rev. D* **102**, 063015 (2020), arXiv:2006.01509 [astro-ph.HE].
- [32] C. Dreissigacker, R. Sharma, C. Messenger, R. Zhao, and R. Prix, Deep-learning continuous gravitational waves, *Physical Review D* **100**, 10.1103/physrevd.100.044009 (2019).
- [33] C. Dreissigacker and R. Prix, Deep-learning continuous gravitational waves: Multiple detectors and realistic noise, *Phys. Rev. D* **102**, 022005 (2020), arXiv:2005.04140 [gr-qc].
- [34] T. S. Yamamoto and T. Tanaka, Use of Excess Power Method and Convolutional Neural Network in All-Sky Search for Continuous Gravitational Waves, (2020), arXiv:2011.12522 [gr-qc].

- [35] E. Cuoco et al., Enhancing Gravitational-Wave Science with Machine Learning, (2020), arXiv:2005.03745 [astro-ph.HE].
- [36] M. Vallisneri, J. Kanner, R. Williams, A. Weinstein, and B. Stephens, The LIGO Open Science Center, in Journal of Physics Conference Series, Journal of Physics Conference Series, Vol. 610 (2015) p. 012021, arXiv:1410.4839 [gr-qc].
- [37] Ligo open science center, <https://doi.org/10.7935/CA75-FM95>.
- [38] Einstein@Home, <https://www.einsteinathome.org/>.
- [39] Observational Relativity and Cosmology division of the MPI for Gravitational Physics Hannover, <https://www.aei.mpg.de/obs-rel-cos>.